Simplified thermal performance model for the design of a PVT heat exchanger dedicated to solar-assisted heat pump

Valentin Delachaux[(1)(2)], Laetitia Brottier[(1)] and Rachid Bennacer[(2)]

(1) DualSun, Marseille (France)

(2) Université Paris-Saclay, ENS Paris-Saclay, CNRS, LMPS, Gif-sur-Yvette (France)

Abstract

With the aim of designing the most efficient photovoltaic-thermal hybrid solar panel (PVT) dedicated to solar-assisted heat pump, it has been built a simplified steady-state 1D-2D numerical model to compare different solutions from their heat gain factor with the ambient air. It allowed apprehending thermal couplings between the different constituent elements from conductive and/or convective heat transfers, and the different contributions linked with geometry variability. While keeping a global vision of the problem, it has been possible to focus on key choices (number of risers, absorber plate thickness, fin height, number of fins) and find optimum solutions. This work would later benefit from being confronted to experimental results and being completed by dynamic modelling and complete CFD simulations for validation and finer understanding purposes.

Keywords: hybrid solar collectors (PVT), sheet-and-tube, unglazed, heat pump (HP), solar-assisted heat pump, thermal performance, free convection, fin-and-tube, numerical model

1. Introduction and objective

The potential of systems based on the coupling of a water/water heat pump and photovoltaic-thermal hybrid solar panels (PVT) as its low temperature source has been highlighted by research projects at European scale such as Sunhorizon and Integrate, studies (Harrison, 2017), , and market trends with the rise of manufacturers of patented dedicated solutions such OptiSolar (FR3040473B1, 2017), Li-Mithra (EP3270084A1, 2018) and Consolar (WO2018033409A1, 2018),

Indeed, this kind of solution makes better use of the strengths of the PVT (low temperature, electric back-up), is more universal (vs. direct DHW preheating limited to systems regularly supplied with cold water) and allows a much higher coverage rate over the year.

First, the main determinant of the performance of such a coupling is the ambient air heat gain factor of the PVT panel to provide thermal power when the solar radiation is low or even zero. Second, a satisfactory level of heat transfer with the PV panel should be maintained, both to collect heat from the sun and cool down the photovoltaic cells. Thus, as part of our own approach to designing a dedicated hybrid panel with any set of constraints (among which the dimensions of the panel), it is at stake to predict thermal performance indicators for any suggested design.

The main idea is to increase the heat transfer surface between the calorific fluid and the air by adding surface extensions (e.g., fins). Any surface extension corresponds to additional heat transfer which depends on geometry, contact surface, base temperature, and convection air flow. To our knowledge, there is only few literatures which considers such new features on PVT heat exchangers with strong coupling between the conduction and convection regimes. The objective is to understand these coupled thermal behaviours and to find optimums for different heat exchanger geometries.

doi:10.18086/eurosun.2022.07.02 Available at http://proceedings.ises.org

2. Numerical model description

2.1 State-of-the-art

The first step was to write a steady-state 1D-2D numerical model in Python[1] for a basic sheet-and-tube unglazed PVT, either a harp or a meander. It is based on the component called *Type 560* which was developed as part of the Electrical Library by Thermal Energy System Specialist (TESS, 2022). As it is mentioned in (Annis, 2015), this algorithm comes from the Hottel-Whillier models for flat-plate solar heat collectors presented in (Duffie and Beckman, 1991) and adapted in (Florschuetz, 1979). Then in (Lovvik and Bergene, 1995) it was developed a very similar but more detailed steady-state model to predict the performance of water-type PVT.

Our model roughly corresponds to the steady-state 2D model of (Zondag et al., 2002). It developed and validated a 3D dynamical model and three steady state (3D, 2D and 1D) models of a double-glazed PVT collector. As in the following, the electric modelling was based on the power coefficient approach to correct the power production at different temperatures. Numerical data agreed with experimental ones within 5%. For the calculation of the daily yield, the simple 1D model performed almost as good as 3D dynamic model.

Another work (Chow, 2003) presented an explicit dynamic thermal model (for a single-glazed flat plat PVT) suitable for system simulation with the control-volume finite difference approach (the PVT panel is assimilated to a network of characteristic volumes) to generate results for hourly performance analysis and provide information on the transient performance. This model was later updated and validated by (Bhattarai et al., 2012) through a comparison with experimental data. It was found that the maximum differences between the measured and predicted values was 1.17 K for water temperature at collector outlet, 2% for collector thermal efficiency and 0.2% for collector electrical efficiency.

A dynamic model was developed on Matlab in (Guarracino et al., 2016) for unglazed, single glazed and double-glazed sheet-and-tube PVT collector. The model assumed constant temperature along the layer thickness (1D along the z direction) but variable temperature along the layer plane (2D finite element method on the x-y plane). In our paper, such 2D aspect is considered only for the absorber sheet through a fin heat conduction analytical solution; for the other layers, the average temperature on the plane is computed. The Matlab model was validated both in steady-state and in dynamic conditions against third party available data. An agreement within ± 8% for fluid temperature difference and thermal efficiency in steady-state conditions was found, whereas in dynamic condition the model was able to compute the time constant of the PVT collector tested by (Amrizal et al., 2013) very closely. Later, this dynamic model was used and integrated in (Sredenšek et al., 2021) for describing the entire photovoltaic/thermal system with a specific thermal energy storage tank; then validated against measurements data on a dedicated experimental system.

In (Simonetti et al., 2018), it went a step further: (i) considered all the layers (the maximum ever: 11) and materials that are used to build the PVT collector, (ii) used the five parameters electric equivalent approach to account for PV power production introducing a more physical way to deal with PV cell connection in series, and (iii) modelled the heat transfer between the tube and the coolant fluid with a fin behavior. Moreover, differently from previously published papers, the validation of the model was carried out considering both "slow variation" and "steep variation" of working conditions and under clear sky and cloudy sky days. This allowed to stress the model and put in evidence its limitations.

2.2 Dedicated steady-state 1D-2D numerical model

In the following, the model is chosen to be suitable for implementation of different types of surface extension and geometries. The objective is to compare their average thermal performance so that the steady-state simulation is adequate. The PV panel is segmented in the direction parallel to the tubes. Each "slice" i corresponding to one tube is considered separately which is legitimized by symmetry assumptions. If the heat exchanger is a meander, these slices are in series, if it is a harp, they are in parallel. It has been kept as an option to slice the panel perpendicular to the tubes depending on the location of the fins.

[1] https://github.com/valentindelachaux/PVT-thermal-performance-model

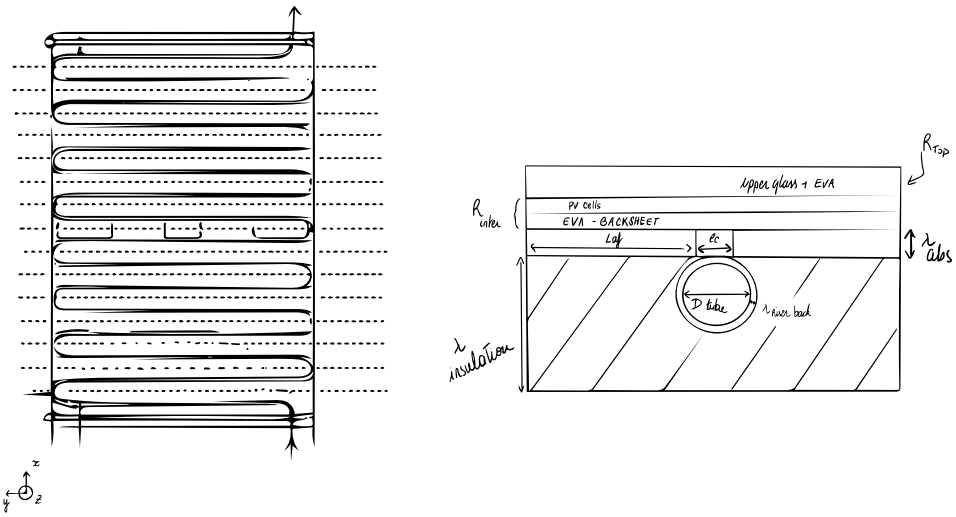

Fig. 1: basic sheet-and-tube PVT panel, the heat exchanger is a meander with horizontal manifolds

These main assumptions – common in the literature mentioned above – are listed below:

- the layers are thin enough to consider temperature constant along each layer thickness: the model is 1D in z direction,
- for any layer except the absorber sheet, the temperature considered is the mean temperature across the x-y plane,
- temperature gradients in the direction of flow and between the tubes can be treated independently: for the absorber sheet, the x-dependency of the temperature is considered while it is averaged along y-direction. Moreover, even if in the case of a meander, the temperature profile between two adjacent pipes is symmetrical and the temperature has a maximum on the symmetrical axis,
- the side effects are not considered,
- the optical properties of all relevant materials are constant,
- all material properties are presumed to be independent of temperature and equal on both sides,
- water flow rate is evenly distributed between the pipes and the thermal losses and mixing effects at the inlet and outlet manifolds are negligible,
- the flow is fully developed in tubes,
- the headers cover a small area of the collector and its effect on the temperature distribution on the absorber can be neglected,
- the incident irradiance G, the wind speed and the ambient temperature are uniform boundary conditions at the surface of the PVT collector,
- it is assumed that there is no dust or partial shading on the collector,
- the reflection, absorption and transmission factors are calculated only for the incident solar irradiance.

Our model uses the notations of the *Type 560* component. Here is the main nomenclature:

Tab. 1: Nomenclature

β	slope of the collector surface	Eff_T	coefficient for the PV cell efficiency as a function of the cell temperature
ε	emissivity	Eff_G	coefficient for the PV cell efficiency as a function of the incident radiation
θ_L	longitudinal angle of incidence	IAM	incidence angle modifier
θ_T	transversal angle of incidence	k	thermal conductivity

λ	thickness of a layer	$R_{abs,back}$	resistance to heat transfer from the absorber to the ambient air at the back of the collector (insulation + convection)
$\tau\alpha$	transmittance-absorptance product for the solar collector	$R_{tube,back}$	resistance to heat transfer from the tube to the ambient air at the back of the collector (insulation + convection)
χ	resistance to heat transfer from the tube to the internal fluid	R_{ins}	resistance provided by the insulation
A_G	gross collector area	R_{inter}	resistance to heat transfer from the PV cells to the absorber plate
C_p	specific heat of the fluid flowing through the PV/T collector	R_{top}	resistance to heat transfer from the upper glass + EVA to the PV cells
C_B	the conductance between the absorber plate and the bonded tube	R_{tube}	resistance provided by the thickness of the tube

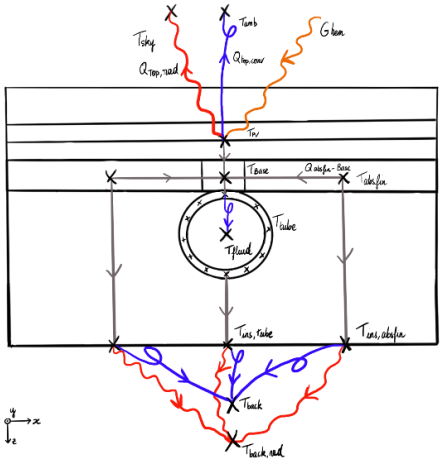

Fig. 2: vertical cross-section of a slice of the PVT panel and diagram of temperature nodes and heat transfers

Let us recall the equations obtained from four energy balances in order to understand how the model is modified to consider the addition of fins.

Energy balance on the PV cells layer

Neglecting conduction along the surface, the energy balance at any point along the surface gives:

$$S = \frac{T_{PV}-T_{amb}}{R_{top}} + h_{rad}\left(T_{PV} - T_{sky}\right) + \frac{T_{PV}-T_{abs}}{R_{inter}} \qquad \text{(eq. 1)}$$

where $T_{PV} = \overline{T_{PV}}^{x,y}$ and $T_{abs} = \overline{T_{abs}}^{x,y} = \frac{l_c \overline{T_B}^{y} + L_{af}\overline{T_{absfin}}^{y}}{W}$

S is the net absorbed solar radiation i.e., the total absorbed solar radiation minus the PV power production:

$$S = (\tau\alpha)_{\theta_L,\theta_T} G_{hem}(1-\eta_{PV}) \qquad \text{(eq. 2)}$$

$(\tau\alpha)_{\theta_L,\theta_T} = IAM(\tau\alpha)_n$ is the transmittance-absorptance product at an angle of incidence (θ_L, θ_T) and should be estimated with the appropriate optical model.

The conversion efficiency η_{nom} of the incident sunlight into electricity is assumed to decrease linearly with increasing cell operating temperature T_{PV}. The electrical model used is the most common one, the power coefficient approach:

$$\eta_{PV} = \eta_{nom}\left(1 + \mathrm{Eff}_T\left(T_{PV} - T_{ref}\right)\right)\left(1 + \mathrm{Eff}_G\left(G_T - G_{ref}\right)\right) \quad \text{(eq. 3)}$$

The PV cells layer transfers heat with the ambient air through the layers above it (glass, EVA) and by convection. The latter is represented by a heat transfer coefficient h_{top} which is calculated for mixed-regime as in (Guarracino et al., 2016) or (Simonetti et al., 2018):

$$h_{top} = \left(h_{free}^3 + h_{forced}^3\right)^{1/3} \quad \text{(eq. 4)}$$

For the upper side of the panel, h_{free} follow these correlations (replacing g by $g\cos(\beta)$ in the Ra number):

Tab. 2: Correlations for the free convection heat transfer coefficient between the upper side of a hot or a cold plate and the ambient air

Name	Case	Validity conditions	Formula
(Churchill and Chu, 1975)	Hot plate	$\beta \geq 45°$ and laminar flow $(10^4 \leq Ra_L \leq 10^9)$	$Nu_L = 0.68 + 0.67Ra_L^{1/4}\left[1 + \left(\frac{0.492}{Pr}\right)^{\frac{9}{16}}\right]^{-\frac{4}{9}}$ (eq. 5)
(Churchill and Chu, 1975)	Hot plate	$\beta \geq 45°$ and turbulent flow $(Ra_L \geq 10^9)$	$Nu_L = 0.10Ra_L^{1/3}$ (eq. 6)
Raithby and Hollands in (Rohsenow et al., 1998)	Hot plate	$\beta < 45°$, $0.024 \leq Pr \leq 2000$, and $Ra_L \geq 10^7$	$Nu_L = 0.14Ra_L^{1/3}\frac{1+0.0107Pr}{1+0.01Pr}$ (eq. 7)
(Fujii and Imura, 1972)	Cold plate	$\beta \geq 2°$ and $(10^5 \leq Ra_L \leq 10^{11})$	$Nu_L = 0.68 + 0.67Ra_L^{1/4}\left[1 + \left(\frac{0.492}{Pr}\right)^{\frac{9}{16}}\right]^{-\frac{4}{9}}$ (eq. 8)

The same correlations are used for the free convection heat transfer coefficient between the lower side of such a plate and the ambient air, by reversing the "hot" and "cold" cases. So they are used for h_{back} computation as well. See the Github repository documentation for the modelling of forced convection at the front.

The radiative heat transfer coefficient is designed to respect the Stefan-Boltzman law:

$$h_{rad} = \varepsilon_{PV\ cells}\sigma\left(T_{PV} + T_{sky}\right)\left(T_{PV}^2 + T_{sky}^2\right) \quad \text{(eq. 9)}$$

(Guarracino et al., 2016) stated that the common model for T_{sky} from (Duffie and Beckman, 1991) (usually valid for clear sky conditions) would lead to less than 1% of error for the value of the collector thermal and electrical output.

$$T_{sky} = 0.0552T_{amb}^{1.5} \quad \text{(eq. 10)}$$

In an ISO/DIS 9806 steady-state indoor test, there is an artificial cold sky so that $T_{sky} = T_{amb}$

Energy balance equation on the "absorber-fin"

The absorber above the tube is considered as two symmetrical fins of length L_{af} with conduction along x-direction. On each side of the absorber-base, the following differential equation for the temperature profile at a given y is found:

$$k_{abs}\lambda_{abs}\frac{d^2T_{abs}}{dx^2} = \frac{T_{abs} - T_{amb}}{R_{abs,back}} - \frac{T_{PV} - T_{abs}}{R_{inter}} \quad \text{(eq. 11)}$$

With these boundary conditions:

$$\begin{cases} T_{abs}\left(x = L_{af}\right) = T_B \\ \frac{dT_{abs}}{dx}(x = 0) = 0 \text{ (symmetry)} \end{cases} \quad \text{(eq. 12)}$$

This equation is solved below:

$$T_{abs}(x, y) = \frac{b}{j} + a_{abs}(y) \times \cosh(mx)$$

with $a_{abs}(y) = \frac{1}{\cosh(mL_{af})}\left(T_B(y) - \frac{b}{j}\right)$ and $m = \sqrt{\frac{F\prime j}{k\lambda}}$ (eq. 13)

At a given y in the fluid direction, $T_{abs}(x) = \overline{T_{abs}}^{y}(x) = \frac{b}{j} + \overline{a_{abs}(y)}^{y} \times \cosh(mx)$ (eq. 14)

With the following parameters:

$F' = \frac{1}{h_{rad}R_{inter} + \frac{R_{inter}}{R_{top}} + 1}$; $b = S + h_{rad}T_{sky} + \frac{T_{amb}}{R_{top}} + \frac{T_{back}}{R_{abs,back}F'}$; $j = \frac{1}{R_{inter}F'} + \frac{1}{R_{abs,back}F'} - \frac{1}{R_{inter}}$ (eq. 15)

Energy balance on the absorber-base

$l_B = l_c + \iota$ is the width of the base of the fin. l_c is the width of the weld. An energy balance on the base (non-fin) area of the absorber plate shows:

$$q'_{Base-tube} = l_c \frac{T_{PV} - T_B}{R_T} - \iota \frac{T_B - T_{back}}{R_{abs,back}} + 2q'_{absfin} \quad \text{(eq. 16)}$$

Assuming $T_B = b_1 q'_{tube-fluid} + b_2 T_{fluid} + b_3 T_{back}$, we get:

$$q'_{Base-tube} = -\theta_{Bt} q'_{tube-fluid} + \kappa_{Bt} T_{fluid} + \epsilon_{Bt} \quad \text{(eq. 17)}$$

Energy balance on the tube

$$q'_{tube-fluid} = q'_{Base-tube} - q'_{tube-back} = C_B(T_B - T_{tube}) - \gamma_{back}(T_{tube} - T_{back}) \quad \text{(eq. 18)}$$

With $C_B = \frac{l_c k_{riser}}{\lambda_{riser}}$ and $\gamma_{back} = \frac{p_{ext,tube}}{R_{tube} + R_{tube,back}} + h_{back,rad} p_{ext,tube,rad}$

The Millman's theorem gives c_1, c_2, and c_3 in $T_{tube} = c_1 T_B + c_2 T_{fluid} + c_3 T_{back}$ and then find b_1, b_2, and b_3. In this calculation, we need $\chi = \frac{1}{h_{fluid} p_{int,tube}}$ and so the internal heat transfer coefficient h_{fluid}. We chose the correlation from (Taler and Taler, 2017) which is valid for $Pr \in [0.6,160]$, $Re \geq 10^4$ and $L/d_w \geq 60$:

$$h_{fluid} = \frac{k_{fluid} Nu}{D_{tube}} \; with \; Nu = 0.023 Re^{0.8} Pr^n, n = 0.7 \quad \text{(eq. 19)}$$

Substituting $q'_{Base-tube}$ from (eq. 17) into (eq.18), we find the heat transfer to fluid (per unit of length in the fluid direction in W/m) as a function of T_{fluid} with three key parameters:

$$q'_{tube-fluid}(y) = \frac{\kappa_{tf}}{\theta_{tf}} T_{fluid}(y) + \frac{\epsilon_{tf}}{\theta_{tf}} \quad \text{(eq. 20)}$$

See the GitHub repository documentation for the expression of κ_{Bt}, θ_{Bt}, ϵ_{Bt}, (b_i), (c_i), κ_{tf}, θ_{tf}, and ϵ_{tf}.

Energy balance on a differential section of fluid moving through the tube

$$\frac{\dot{m} C_p}{N_{harp}} \frac{dT_{fluid}}{dy} = q'_{tube-fluid}$$
(eq. 21)

$$\frac{dT_{fluid}}{dy} = a_f T_{fluid} + b_f \text{ where } \begin{cases} a_f = \frac{N_{harp}}{\dot{m} C_p} \frac{\kappa_{tf}}{\theta_{tf}} \\ b_f = \frac{N_{harp}}{\dot{m} C_p} \frac{\epsilon_{tf}}{\theta_{tf}} \end{cases} \quad \text{(eq. 22)}$$

Finally, we get the temperature field of the fluid in the tube:

$$T_{fluid}(y) = \left(T_{fluid,in} + \frac{b_f}{a_f}\right) \exp(a_f y) - \frac{b_f}{a_f} \quad \text{(eq. 23)}$$

Likewise, see the GitHub repository documentation to find the expression of the average temperature of the fluid along the tube $\overline{T_{fluid}}$, the heat transfer q'_{fluid}, the average temperature of the base of the absorber along the tube $\overline{T_B}$, the average temperature of the absorber-fin on either side of the tube $\overline{T_{absfin}}$, the average temperature of the absorber $\overline{T_{abs}}$ and the average temperature of the PV cells layer $\overline{T_{PV}}$.

The solution of this set of equations requires an iterative approach until convergence.

2.3 Implementation of fins

The second step consisted in the implementation of surface extensions in these equations. They are either against tubes (e.g., a fin-and-tubes heat exchanger usually found as a heat pump evaporator, a finned-tubes heat exchanger) or against the absorber plate. In the latter, fins are in series with the "absorber-fin".

Fins welded on the tubes (f0) and (f1)

The fins (f0) are welded vertical against the tubes, and perpendicular to the fluid direction y, so that they are parallel to the free convection air flow. Each fin is characterized by the number of Biot $Bi = \left(1 + \frac{\lambda_{fin}}{\delta_{fin}}\right)\frac{\lambda_{fin} h_{back}}{k_{fin}}$.

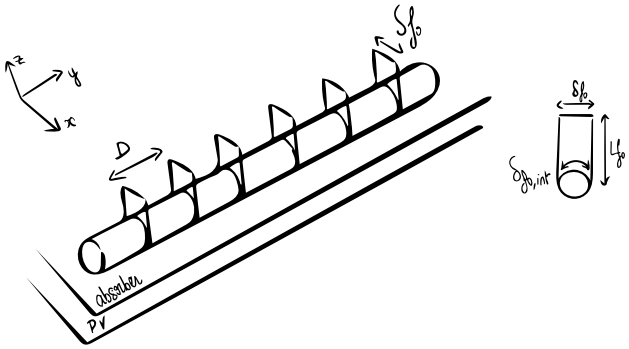

Fig. 3: vertical fins welded perpendicular to the tubes (f0)

Here is the heat equation:

$$\frac{d^2 T_{fin}}{dx^2} - \frac{2Bi}{\lambda_{fin}^2}\left(T_{fin}(x) - T_{ext}\right) = 0 \qquad \text{(eq. 24)}$$

Boundary conditions if symmetry or zero-flux end:

$$\begin{cases} T_{fin}(x = 0) = T_{tube}(y) \\ \frac{d}{dt} T_{fin}\left(x = L_{fin}\right) = 0 \end{cases} \qquad \text{(eq. 25)}$$

Boundary conditions if free-flux end:

$$\begin{cases} T_{fin}(x = 0) = T_{tube}(y) \\ k\frac{dT_{fin}}{dz}\left(z = L_{fin}\right) = -h_{back}\left(T_{fin}\left(z = L_{fin}\right) - T_{back}\right) \end{cases} \qquad \text{(eq. 26)}$$

Solving this equation requires the computation of γ, fin and flow characteristic number:

$$\gamma = \frac{\frac{\alpha}{\lambda_{fin}}\sinh\left(\frac{\alpha}{\lambda_{fin}}L_{fin}\right) + \frac{\beta\alpha}{\lambda_{fin}}\cosh\left(\frac{\alpha}{\lambda_{fin}}L_{fin}\right)}{\cosh\left(\frac{\alpha}{\lambda_{fin}}L_{fin}\right) + \beta\sinh\left(\frac{\alpha}{\lambda_{fin}}L_{fin}\right)} \text{ with } \alpha = \sqrt{2Bi} \text{ and } \beta = \frac{\sqrt{Bi/2}}{\left(1 + \frac{\lambda_{fin}}{\delta_{fin}}\right)}$$

(eq. 27)

Without detailing it here, horizontal fins (f1) welded from one tube to the other have been modelled as well. For a slice *i* of the panel, at a given *y*, the average heat transfer through the fins on back and on either side is:

$$q_{f0}' = \gamma_0^{int}(T_{tube}(y) - T_{back}) \text{ with } \gamma_0^{int} = k_{f0}\gamma_0 \frac{\lambda_{f0} N_{f0} \delta_{f0}^{int}}{L_{tube}} \qquad \text{(eq. 28)}$$

$$q_{f1}' = \gamma_1^{int}(T_{tube}(y) - T_{back}) \qquad \text{with } \gamma_1^{int} = 2k_{f1}\frac{\lambda_{f1} N_{f1} \delta_{f1}^{int}}{L_{tube}} \frac{\sqrt{2Bi_{f1}}}{\lambda_{f1}} \tanh\left(\sqrt{2Bi_{f1}}\frac{L_{f1}}{\lambda_{f1}}\right) \qquad \text{(eq. 29)}$$

Then, we adapt the model with these additional heat transfers:

$$\gamma_{back} \leftarrow \gamma_{back} + \gamma_0^{int} + \gamma_1^{int} \qquad \text{(eq. 30)}$$

Fins welded on the absorber plate (f2)

These are also vertical and perpendicular to the fluid direction y.

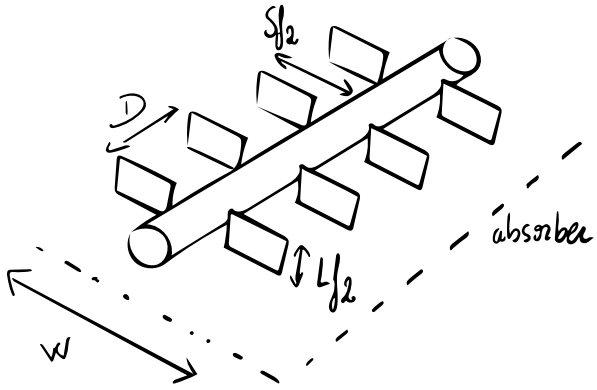

Fig. 4: vertical fins welded on the absorber plate, perpendicular to the tubes (f2)

For half of the fin on one side of the tube, the heat transfer in $W/(m^2 of contact)$ is:

$$q_{f2} = \gamma_2^{int}\left(\overline{T_{abs}}^{y}(x) - T_{back}\right) \text{ with } \gamma_2^{int} = k\gamma_2 \frac{\lambda_{f2} N_{f2} \delta_{f2}}{L_{tube}\delta_{f2}} \quad \text{(eq. 31)}$$

The b and j coefficients from $T_{abs}(x) = \overline{T_{abs}}^{y}(x) = \frac{b}{j} + \left(T_B(y) - \frac{b}{j}\right)\frac{\cosh(mx)}{\cosh(mL_{af})}$ become:

$$b \leftarrow b + \frac{\gamma_2^{int} T_{back}}{F'} \qquad j \leftarrow j + \frac{\gamma_2^{int}}{F'} \quad \text{(eq. 32)}$$

3. Methodology

We developed a numerical model which predicts the steady-state thermal power output of one PVT panel under a set of meteorological (irradiance, ambient temperature, wind) and system parameters (inlet fluid temperature, flow rate). By running this simulation into a sample of test data, so it is possible to get the a_i coefficients which characterize the panel according to (eq. 42) from ("ISO/DIS 9806:2017 Solar energy — Solar thermal — Test methods," 2017).

$$\dot{Q} = A_G\left(\eta_{0,hem} K_{hem} G - a_1(T_m - T_a) - a_2(T_m - T_a)^2 - a_3 u'(T_m - T_a) + a_4 G' - a_6 u' G - a_7 u' G' - a_8(T_m - T_a)^4\right) \quad \text{(eq. 33)}$$

Since the latest version of this standard, the coefficients a_2 and a_8 are often set to zero for PVT panels because the thermal power is considered linearly dependent on the temperature difference. Besides, the heat exchanger being in a narrow space between the panel and the roof, it has been assumed that the wind does not modify the convective heat transfers on the rear side. Therefore, the information of geometry impact on free convection air flow is contained only in the a_1 coefficient. The information of forced convection impact is theoretically contained only in a_3.

In the following, the optical efficiency $A0 = a_0 - a_6 u'$ and the heat loss coefficient $A1 = a_1 + a_3 u'$ are retained as the two main thermal performance representative values. An average wind speed of u = 1.3 m/s is assumed so that u' = -1.7 m/s.

This model includes modelling temperature fields in and over the constituent elements of the exchanger and fluid flow geometry (having an impact on internal heat transfer coefficient and temperature field along its path). It allows analysing the different contributions by heat transfer type (conduction, convection, radiation) and by source (sun irradiance, ambient air) linked with geometry variability and finding optimum solutions.

In the following, we analyse a basic PVT prototype. We do not consider the manifolds. We use our numerical model directly without calibration following the experimental tests

4. Results

4.1. Number of risers

A specific PVT panel prototype has been studied. The heat exchanger is a meander made up with 16 risers bonded against an aluminum absorber sheet. The latter is plated against the backsheet of the PV panel.

Tab. 3: PVT panel prototype characteristics

Parameter	Symbol	Value
Nominal efficiency	η	20%
Power decrease coefficient	Eff_T	-0.0034 /K
Tilt	β	45°
Number of risers	N	16
Gross area	A_G	1.93 m^2
Absorber length	L_{abs}	1,550 mm
Absorber width	w_{abs}	1,080 mm
Tube diameter	D_{tube}	8 mm
Weld width	l_c	4 mm
Absorber conductivity	k_{abs}	226 W/mK
Absorber thickness	λ_{abs}	0.4 mm

A greater number of risers makes it possible to collect heat transfer from the absorber more efficiently. Above a certain number, the absorber surface associated with each tube is sufficiently small for a major part of these transfers to be collected. Note that we are in the case of a meander exchanger, the flow rate is therefore constant, as is the internal heat transfer coefficient of the fluid.

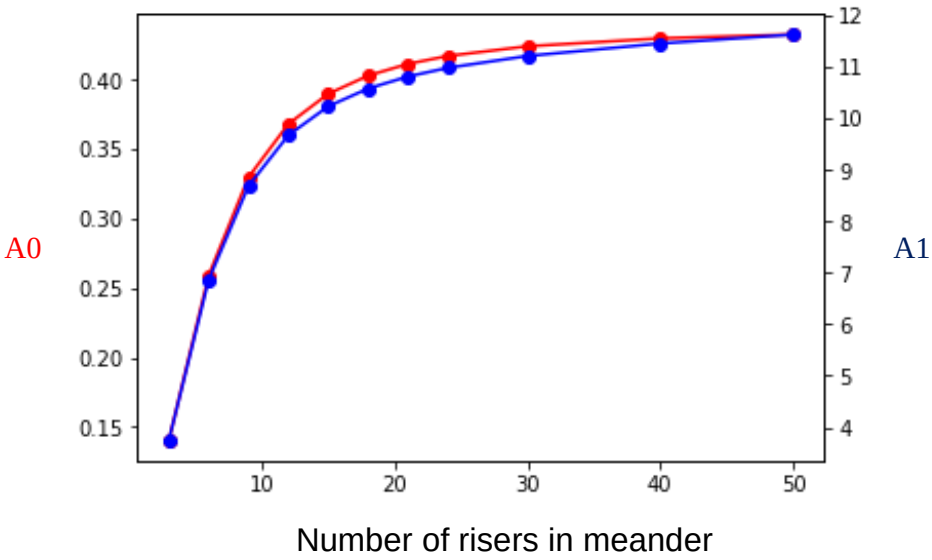

Fig. 5: A0 and A1 (for u = 1,3 m/s) dependency on the number of risers for our meander PVT panel

4.2 Absorber thickness

The absorber, on either side of each tube, acts as a fin:

- One face being in direct contact with the backsheet, transmits the heat from sunlight, radiative transfer, and convection on the upper side
- The other side transmits the heat from convection on the lower side

This function makes it possible to exploit the entire surface of the collector. To improve A0 and A1 coefficients, the fin must therefore play its role as well as possible.

With the same panel, here is a parametric study about the absorber plate thickness. Indeed, it behaves like a fin on each side of each tube, so its conductance (product of thermal conductivity and thickness) is highly influent on thermal performance.

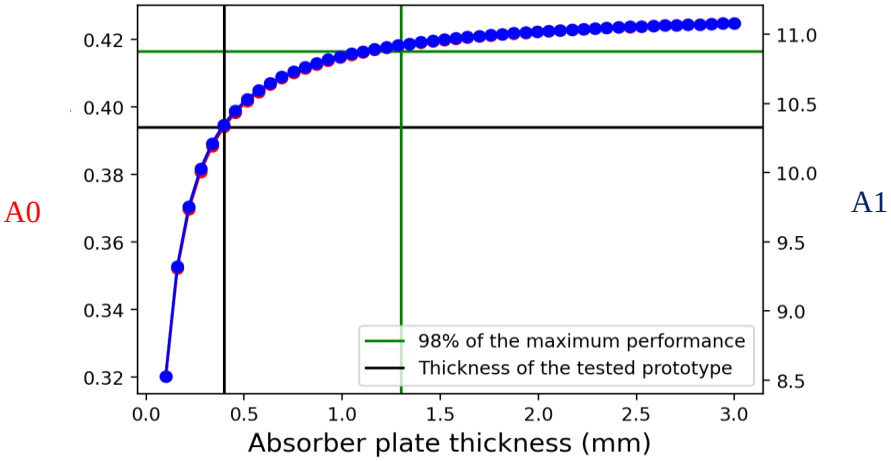

Fig. 6: A0 and A1 (for u = 1,3 m/s) dependency on absorber plate thickness for our meander PVT panel

It is found that the aluminum absorber plate should have a thickness of at least 1.3 mm to get a minimum of 98% of the maximum value reached for about 27 mm of thickness. If the absorber plate of the prototype is replaced by a 1.3 mm-thick one, the A0 would increase by about 3 points which corresponds to about 7% more energy produced every year.

4.3. Fins height L

Tab. 4: PVT panel prototype characteristics

Number of fins	N_{f2}	120
Fin spacing	D	9 mm
Fins conductivity	k_{f2}	226 W/mK
Fins thickness	λ_{f2}	1.5 mm

As shown above, the behavior of rectangular vertical fins plated on the absorber is known with an analytical solution giving the incoming heat flux at the base of each fin according to their geometry. Specifically, the influence of their height L is well known. It significantly increases the heat flux until some point. Beyond the threshold value of $L < \frac{\sqrt{ka}}{h}$, the rest of the fin is "useless". Here the calculated threshold value with an average rear side heat transfer coefficient of h = 3,6 W/m^{2}K is about 31 cm. The simulation for this PVT panel, with fins perpendicular to the tubes and plated against the absorber plate, reflects this phenomenon, and gives approximate expected values for the performance indicators A0 and A1.

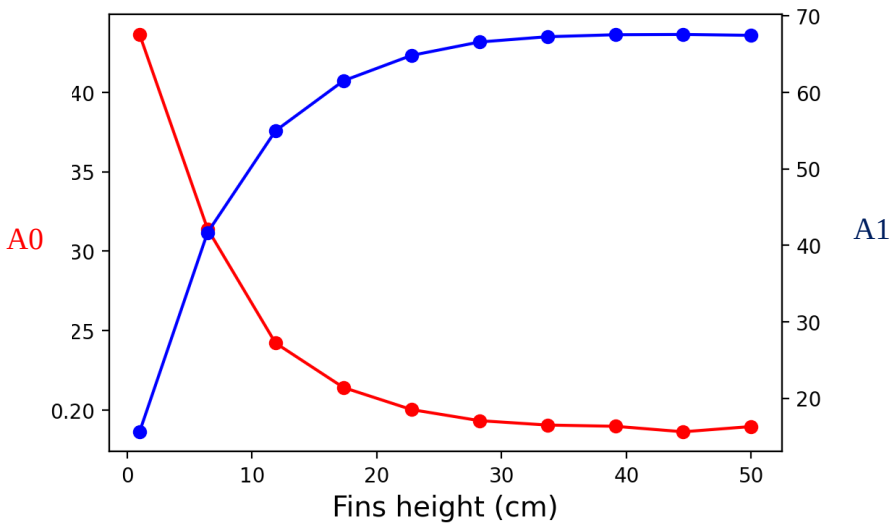

Fig. 7: A0 and A1 (for u = 1,3 m/s) dependency on fins height for the PVT panel with fins perpendicular to the tubes and plated against the absorber plate (120 aluminum fins, 1.5 mm thick, fin spacing of 9 mm,)

4.4. Fins number

Tab. 4: PVT panel prototype characteristics

Fins length	L_{f0}	20 mm
Fins width	δ_{f0}	10 mm
Contact width between fins and tube	δ_{f0}^{int}	$(\pi D_{tube})/2$ = 13 mm

As another example, the PVT heat exchanger has fins perpendicular to the tubes and welded against them. A key choice, in such a design, is the number of fins (i.e., the fin spacing) because it negatively influences the heat transfer coefficient on the back of the panel h_{back} as (Tari and Mehrtash, 2013) shows. It dealt with free convection heat transfer from plate-fin heat sinks and gave a complete set of Nusselt number correlations covering all inclination angles. As Fig. 8 shows, it allows finding the optimum fin spacing to maximize the global heat loss coefficient A1 or optimizing the number of fins against weight and/or cost constraints.

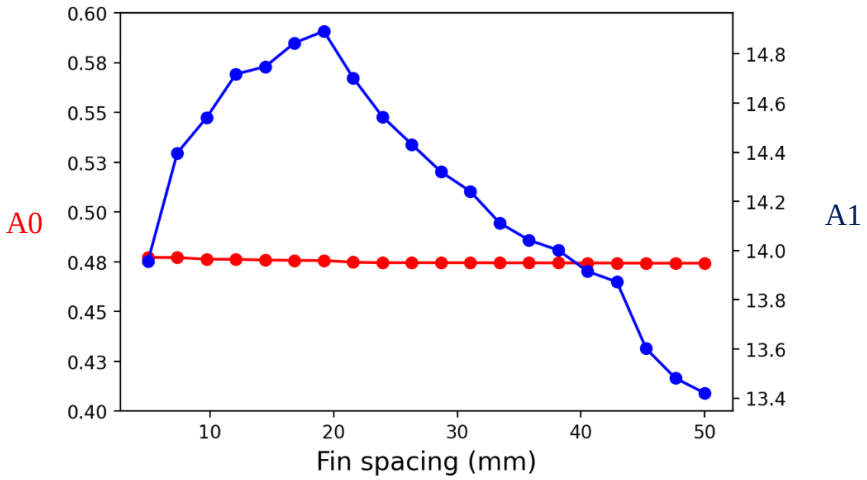

Fig. 8: A0 and A1 (for u = 1,3 m/s) dependency on fin spacing for the PVT panel with fins perpendicular to the tubes and welded against them (52 mm long fins, 1.5 mm thick)

5. Conclusion

This model allowed us to study thermal performance of a variety of heat exchanger pre-designs and understand the determinants of different contributions. While keeping a global vision of the problem, it has been possible to focus on key choices and find optimum solutions for the number of tubes, the absorber thickness, the fins height or spacing. In our approach, the model has been assumed to be relevant to compare geometries with each other. First, it would benefit from being confronted with experimental results. Indeed, quantification of uncertainties is at stake as (Huang and Shah, 1992) showed. Second, a dynamic modelling of thermal performance would complete the analysis, e.g. by adapting the model of (Guarracino et al., 2016). Third, CFD simulations could contribute to the validation of optimizations and to the understanding of thermal couplings with the consideration of temperature inhomogeneities, as shown in (Singh et al., 2015), (Taler et al., 2019) and (Marcinkowski et al., 2021). It has been shown that the impact of the heat exchanger geometry, the frame of the panel, and the incidence angle on the free convection air flow should be studied to optimize such a PVT panel dedicated to a solar-assisted heat pump.

6. References

Amrizal, N., Chemisana, D., Rosell, J.I., 2013. Hybrid photovoltaic–thermal solar collectors dynamic modeling. Appl. Energy 101, 797–807. https://doi.org/10.1016/j.apenergy.2012.08.020

Annis, N.C., 2015. Performance analysis and modelling of hybrid photovoltaic-thermal solar panels.

Bhattarai, S., Oh, J.-H., Euh, S.-H., Krishna Kafle, G., Hyun Kim, D., 2012. Simulation and model validation of sheet and tube type photovoltaic thermal solar system and conventional solar collecting system in transient states. Sol. Energy Mater. Sol. Cells 103, 184–193. https://doi.org/10.1016/j.solmat.2012.04.017

Chow, T.T., 2003. Performance analysis of photovoltaic-thermal collector by explicit dynamic model. Sol. Energy 75, 143–152. https://doi.org/10.1016/j.solener.2003.07.001

Churchill, S.W., Chu, H.H.S., 1975. Correlating equations for laminar and turbulent free convection from a vertical plate. Int. J. Heat Mass Transf. 18, 1323–1329. https://doi.org/10.1016/0017-9310(75)90243-4

Duffie, J.A., Beckman, W.A., 1991. Solar Engineering of Thermal Processes 928.

Florschuetz, L.W., 1979. Extension of the Hottel-Whillier model to the analysis of combined photovoltaic/thermal flat plate collectors. Sol. Energy 22, 361–366. https://doi.org/10.1016/0038-092X(79)90190-7

Fujii, T., Imura, H., 1972. Natural-convection heat transfer from a plate with arbitrary inclination. Int. J. Heat Mass Transf. 15, 755–767. https://doi.org/10.1016/0017-9310(72)90118-4

Guarracino, I., Mellor, A., Ekins-Daukes, N.J., Markides, C.N., 2016. Dynamic coupled thermal-and-electrical modelling of sheet-and-tube hybrid photovoltaic/thermal (PVT) collectors. Appl. Therm. Eng. 101, 778–795. https://doi.org/10.1016/j.applthermaleng.2016.02.056

Harrison, S., 2017. The Potential and Challenges of Solar Boosted Heat Pumps for Domestic Hot Water Heating. Presented at the 12th IEA Heat Pump Conference, Rotterdam.

ISO/DIS 9806:2017 Solar energy — Solar thermal — Test methods, 2017.

Lovvik, O.M., Bergene, T., 1995. Model calculations on a flat-plate solar heat collector with integrated solar cells 10.

Marcinkowski, M., Taler, D., Taler, J., Węglarz, K., 2021. Thermal Calculations of Four-Row Plate-Fin and Tube Heat Exchanger Taking into Account Different Air-Side Correlations on Individual Rows of Tubes for Low Reynold Numbers. Energies 14, 6978. https://doi.org/10.3390/en14216978

Rohsenow, W.M., Hartnett, J.P., Cho, Y.I. (Eds.), 1998. Handbook of heat transfer, 3rd ed. ed, McGraw-Hill handbooks. McGraw-Hill, New York.

Simonetti, R., Molinaroli, L., Manzolini, G., 2018. Development and validation of a comprehensive dynamic mathematical model for hybrid PV/T solar collectors. Appl. Therm. Eng. 133, 543–554. https://doi.org/10.1016/j.applthermaleng.2018.01.093

Singh, S., Sørensen, K., Condra, T., 2015. Multiphysics Numerical Modeling of a Fin and Tube Heat Exchanger. Presented at the The 56th Conference on Simulation and Modelling (SIMS 56), October, 7-9, 2015, Linköping University, Sweden, pp. 383–390. https://doi.org/10.3384/ecp15119383

Sredenšek, K., Seme, S., Štumberger, B., Hadžiselimović, M., Chowdhury, A., Praunseis, Z., 2021. Experimental Validation of a Dynamic Photovoltaic/Thermal Collector Model in Combination with a Thermal Energy Storage Tank. Energies 14, 8162. https://doi.org/10.3390/en14238162

Taler, D., Taler, J., 2017. Simple heat transfer correlations for turbulent tube flow. E3S Web Conf. 13, 02008. https://doi.org/10.1051/e3sconf/20171302008

Taler, D., Taler, J., Wrona, K., 2019. Transient behavior of a plate-fin-and-tube heat exchanger taking into account different heat transfer coefficients on the individual tube rows. E3S Web Conf. 137, 01036. https://doi.org/10.1051/e3sconf/201913701036

Tari, I., Mehrtash, M., 2013. Natural convection heat transfer from horizontal and slightly inclined plate-fin heat sinks. Appl. Therm. Eng. 61, 728–736. https://doi.org/10.1016/j.applthermaleng.2013.09.003

TESS, 2022. TESS Component Libraries v18.

Zondag, H.A., de Vries, D.W., van Helden, W.G.J., van Zolingen, R.J.C., van Steenhoven, A.A., 2002. The thermal and electrical yield of a PV-thermal collector. Sol. Energy 72, 113–128. https://doi.org/10.1016/S0038-092X(01)00094-9